IEEE Access
Multidisciplinary | Rapid Review | Open Access Journal

Received 9 October 2023, accepted 28 October 2023, date of publication 6 November 2023, date of current version 21 November 2023.

Digital Object Identifier 10.1109/ACCESS.2023.3330137

RESEARCH ARTICLE

Margin-Maximized Hyperspace for Fault Detection and Prediction: A Case Study With an Elevator Door

MINJAE KIM[1], SEHO SON[1], AND KI-YONG OH[2]
[1]Department of Mechanical Convergence Engineering, Hanyang University, Seondong-gu, Seoul 04763, Republic of Korea
[2]School of Mechanical Engineering, Hanyang University, Seondong-gu, Seoul 04763, Republic of Korea

Corresponding author: Ki-Yong Oh (kiyongoh@hanyang.ac.kr)

This work was supported in part by the Korea Institute of Energy Technology Evaluation and Planning (KETEP) Grant funded by the Korean Government (Ministry of Trade, Industry and Energy, MOTIE), Development of Fire Detection and Protection System for Wind Turbine, under Grant 20213030020260; in part by the KETEP Grant funded by the Korean Government (MOTIE), Development of Intelligent O&M Technologies for Standard Combined Cycle Power Plant, under Grant 20217010100020: and in part by the Research and Development on Fire Safety Technology for ESS Hydrogen Facilities, 20011568, Development of Automatic Extinguishing System for ESS Fire, funded by the National Fire Agency (NFA, Korea).

ABSTRACT This study proposes a practical fault detection and prediction method by addressing a margin-maximized hyperspace. The proposed method is effective for a highly imbalanced dataset without any supervision, which is a frequently occurring and challenging problem in real-world applications. The proposed method has three characteristics. First, knowledge-based feature manipulation is executed to provide sufficient information for a neural network. Second, a regulated variational autoencoder transforms distinct input features into a latent space, which ensures high accuracy and robustness. Third, the obtained latent space is confirmed to statistically allocate two extremes of major (normal) and minor (faulty) clusters at an origin and unity, maximizing the sensitivity to classify faults. The effectiveness of the proposed method is demonstrated through field measurements of elevator door-strokes and showed high sensitivity to separate each cluster along with locational constancy compared to other autoencoders. Therefore, the proposed method is effective for real-world applications with scarce fault measurements.

INDEX TERMS Artificial neural networks, anomaly detection, deep learning, dimensionality reduction, expert systems, fault diagnosis, machine learning, prognostics and health management, support vector machines, unsupervised learning.

I. INTRODUCTION

Fault detection and diagnosis (FDD) on a variety of mechatronics systems, including motors [1], [2], [3], [4], [5], [6], [7], [8], wind turbines [9], [10], automobiles [11], gas turbines [12], [13], [14], and HVAC systems [15], [16], [17], [18] have been investigated worldwide because manufacturers and customers require to minimize the downtime of these systems to reduce operational and maintenance costs [19]. FDD can be classified into three approaches: physics-based, knowledge-based, and data-driven approaches [20]. A physics-based approach is represented by empirical equations and finite element models that derive mathematical equations explaining the physics and inherent nature of a system of interest. Then, the residuals between the predictions from a model and those from a real system determine the current healthy state of the system of interest because a large residual would be a symptom of faults [21]. This method depends less on the amount of data. However, predicting faults originating from highly nonlinear phenomena and dynamics that are not exactly modeled is challenging. Significant computational effort is further required to address the complex dynamics of the system of interest [22]. The knowledge-based approach correlates a fault phenomenon and cause and then uses ontology-reasoning technology for FDD. With this approach, the origin of faults can be fully explained, and actions can be taken to repair or maintain the system properly. However, this approach requires expert sys-

The associate editor coordinating the review of this manuscript and approving it for publication was Gerard-Andre Capolino.

tems containing both domain knowledge about the structure and symptoms of faults [23], suggesting that this method is impractical because the affluent experience of expert systems is expensive and identifying the complex dynamics of an entire system of interest in real-world industries is practically unfeasible. A data-driven approach is more flexible than the other two approaches because this approach learns the complex dynamics and nonlinear phenomena of a system of interest correlated to faults from data or measurements. This approach requires huge data for the complex dynamics and inherent nature of a system of interest [24], suggesting that gathering huge data is a prerequisite for securing the accuracy and robustness of FDD.

Among these approaches, a data-driven approach has been actively studied nowadays because of its flexibility and significant potential for FDD by accounting for all complex dynamics and the nature of the system of interest under the assumption that big data is available. Specifically, the popularity of data-driven methods originates from recent explosive progress and advances in artificial intelligence technology [25]. Data-driven FDD is classified as supervised and semi-supervised or unsupervised learning, where supervised learning aims to classify a healthy state of the system of interest using both input data and associated labels, whereas only input data are provided for unsupervised learning and a few labeled data are given for semi-supervised learning [26]. Semi-supervised or unsupervised learning has become dominant and has attracted significant attention recently because supervised learning requires labeling a total dataset as a prerequisite, which requires one-by-one decisions from expert systems [27]. Labeling an entire dataset is a highly cost-ineffective and practically unrealistic task in industrial applications because huge data are collected every day, and only a few people have the expertise to identify the real condition of a target object based on domain knowledge [28].

Among many semi-supervised or unsupervised learning methods in the data-driven approach, autoencoder (AE), which comprises an encoding layer for compressing the input data and a decoding layer for reconstructing the compressed data as same as the input data [29], has become popular in the field of FDD. The architecture of an AE can identify complex nonlinear correlations among input variables because an AE features strong nonlinear transformation characteristics, where faults are easily detected and classified [30]. Specifically, AE extracts significant information from input data by compressing high-dimensional input data, transforming the features into a low-dimensional latent space, and then reconstructing the compressed features into the same dimension as that of the input data. Hence, features are clearly shown in a latent space because nonlinear space transformation through layers well extract features from input data [31].

Among various types of AE, variational autoencoder (VAE), comprising not only encoding and decoding layers similar to AE but also a sampling layer for featuring statistical distribution in a latent space, has become popular in the field of FDD. This observation can be explained by the fact that the architecture of VAE can compensate data deficiency problem by its data augmentation characteristic, ensuring high robustness compared to conventional AEs [32]. Recently, approaches to solve FDD problems using VAE could be classified into three ways, each one also has its drawbacks. The first and most dominant use of VAE is for alleviating data imbalance levels by generating pseudo data and using them for improving the accuracy of an independent supervised classifier [33], [34], [35]. This approach would be effective because the original distribution is maintained and shows a better generalization effect compared to other linear sampling methods such as the synthetic minority oversampling technique (SMOTE) [36]. However, this approach would be impractical in solving real-world problems because sufficient fault data are required for using a VAE for generating purposes and that amount of data is not approachable in most cases. The second approach is to train the model only with healthy state data and then observe the residuals between raw and reconstructed data. In this approach, the residuals are representative metrics for the abnormality of the machinery [37], [38]. This approach would be suitable for solving real-world problems because any abnormal data are required for training. However, this approach also has its limitations in that cleaning out all the abnormal data from the entire data is extremely time-consuming and requires the domain knowledge of experts. The last approach is to compress high-dimensional input data into low-dimensional latent space and decide each status based on its location in latent space [39], [40], [41], [42]. In general, isolation algorithms including one-class support vector machine (SVM) [39], [40] or other nonlinear classifiers [41], [42] are utilized for making decisions. This approach could be effective because the encoder could extract high-level features related to abnormality while the curse of dimension is alleviated simultaneously [43]. However, this approach also has three downsides. The first one is that entire labels must be approachable for searching a boundary. The second one is that it is impossible to predict faults with such traditional methods when the system shows degradation symptoms, which is the main disadvantage compared to other methods utilizing the exact remaining useful lifetime (RUL) [44], [45]. The last one is that the distribution on the latent space varies with each training, which results in confusion and restricts clear decisions from users [46].

To overcome the limitations in previous studies, this study proposes a margin-maximized hyperspace (MMH), in which effective fault classification and prediction can be executed for a highly imbalanced dataset. This study aims to maximize sensitivity in a featured space for classifying normal (major) and faulty (minor) clusters in unlabeled and highly imbalanced datasets, which is a frequent and challenging issue in real-world applications. Specifically, the proposed method considers VAE from a different perspective other than generative purposes so that the normal and faulty data can be situated in the invariant location even with repetitive

training. The novelty and key contributions of this study are summarized as follows.

- This study proposes knowledge-based feature manipulation. Newly manipulated features contain distinct information that is directly correlated with faults in the system of interest and the combined application of manipulated features and original measurements is effective for classifying faults from normal data.
- The proposed method transforms input features into a nonlinear latent space via a VAE. This architecture enables the input features to be compressed into a low-dimensional latent space, which shows high accuracy and robustness in classifying faults.
- This study proposes MMH, which can be obtained from VAE with restricted latent space and Bayesian optimization. The proposed method maximizes the distance between normal and faulty clusters by locating two clusters to two extremes of origin and unity in the latent space, enabling accurate fault classification and prediction.
- The effectiveness of the proposed method in solving real-world issues is validated with a field measurement of elevator door strokes. This demonstration confirms maximized sensitivity dividing two clusters of normal and fault strokes and locational constancy remaining at the same location, suggesting that the proposed method is highly effective and practical in actual field applications.

The remainder of this paper is organized as follows. Section II explains the proposed method comprising preprocessing, feature extraction, and the detailed principles of the proposed MMH method. Section III describes the details of the experiment comprising data description, model construction, and evaluation index. Section IV presents the results with an in-depth discussion, including the physical characteristics of elevator door faults and fault classification and prediction using the MMH method with field measurements. Section V reemphasizes the novelty of the proposed method and briefly discusses future work.

II. METHODOLOGY

The entire process of the proposed framework comprises three phases (Figure 1). First, the measurements are preprocessed (Phase A in Figure 1) to change the form of datasets from time-series raw data to the form of stroke data, resulting in the formation of inputs for the proposed method. Specifically, data collected below 8 Hz or above 10 Hz were filtered, and the filtered measurements were unified to the same frequency of 10 Hz. Second, features highly correlated to faults, are extracted from the input data in the form of an open/close stroke and transformed into a regulated latent space (Phase B in Figure 1). Three types of statistical features are extracted. Subsequently, the features are passed through a VAE to transform the features into a new two-dimensional latent space. Third, the MMH method is used for fault detection and prediction of an elevator door (Phase C in Figure 1). A marginal distance between two clusters defined by normal and fault is first maximized using Bayesian optimization in the latent space, resulting in MMH. Then, an SVM is applied for fault detection, and the maximized marginal space between two clusters is used for fault prediction by addressing the principle of a distance-based RUL estimator.

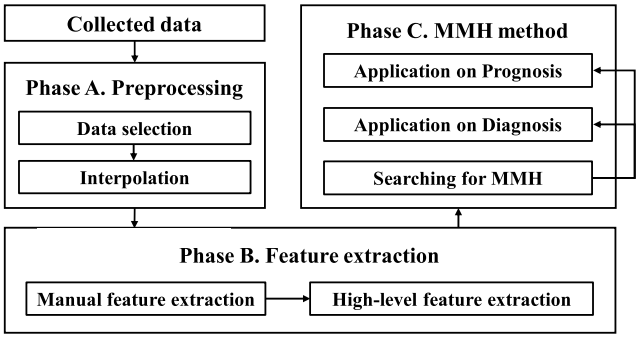

FIGURE 1. Flowchart of the proposed prognosis framework.

A. PREPROCESSING

This phase describes the process of data preprocessing for training and testing. First, measurements were filtered out when the elevator was not in operation and the measurements during the moving operation were also eliminated because this operation did not include data related to the door, which is more than 90% of the total measurements. Next, the refined data were chopped into each stroke because the original time-series data were not appropriate for the proposed neural network. Then the strokes with missing values were excluded from the dataset. These missing values may be caused by an unstable data communication line.

The data in the form of a single stroke were interpolated into the same frequency because the same period of measurements is effective for training the proposed method. The communication load from a controller might have caused the variance in the measuring frequency even though the value was set to 10 Hz. Therefore, measurements recorded below 8 Hz or above 10 Hz were eliminated, and the filtered measurements were interpolated into a single frequency of 10 Hz. Data excluded from this process is only 0.005 % compared to original measurements, suggesting that this data loss is negligible, and characteristics of the measurements after cleaning could represent those of the original operation of an elevator door. Specifically, linear interpolation was executed in this process for real-number-type data, including door position, torque, and speed, whereas nearest interpolation was executed for Boolean-type data such as commands or safety signals.

B. FEATURE EXTRACTION

This phase comprised two major steps. First, manual features were extracted. Specifically, additional features were manipulated from both the torque and speed measurements by subtracting the feedback signals from the reference signals. Subsequently, three types of statistical features were obtained from seven physical properties, including two manipulated

features. Second, high-level features were extracted in a constrained latent space by addressing the VAE. The detailed process of each step is described below.

In the first step, new features were manipulated and normalized. Features highly correlated to motor delay were selected in this study because motor delay, a phenomenon in which the feedback signal is different from a reference signal, usually appears when an anomaly or fault occurs in machinery [47]. This physical interpretation of a fault generally occurs especially in a rotational system, suggesting that the difference between the reference and feedback signals of torque and speed plays a crucial role in inferring the health condition of an elevator door. Therefore, two additional features were added by calculating the differences in the torque and speed measurements. Manipulated features, which are transformed into easier form of learning input features, are effective for training a neural network because the neural network utilized has a limited capacity in consideration of the limited data available [48]. Then, three statistical features, peak, mean, and root-mean-square (RMS), were extracted from measurements at each stroke. Then, the processed data were normalized to improve convergence and to unify their sensitivity to the weights of the neural network. Normalization can be performed by addressing the min-max or Z-score normalization methods [49]. Selecting the best normalization method depends significantly on the data used in the analysis. Therefore, an appropriate normalization method was selected for the data of an elevator door through the optimization of hyperparameters. More details for the optimization process are covered in Section II-C.

In the second step, high-level features were extracted by addressing VAE [32]. A VAE is an advanced AE architecture because it extracts valuable information from a reconstructed space. The most crucial feature of VAE compared to AE is that VAE encodes entire input data into latent space which follows a predefined probabilistic distribution. These characteristics ensure the high robustness of the VAE [50]. In this study, the encoder was trained for latent space to follow a normal distribution $N(\mu, \sigma^2)$. Only means were used to reflect the latent space, whereas standard deviations were limitedly used for sampling variables before passing through the decoder for reconstruction. This architecture would be effective for fault classification and prediction because small perturbations applied at the latent space can compromise a minor variance of input data distribution, which is irrelevant to the health condition of interest.

In this study, means and standard deviations of the latent space were constrained by addressing a sigmoid layer rather than applying the value itself as vanilla VAE does so that each dimension of the latent space was limited to [0, 1]. The constraints enable the latent space to remain within a certain region so that a quantitative comparison is available when a fault is detected and predicted. The variables in the latent space were trained to follow the standard Gaussian distribution $N(0, 1)$. Therefore, the latent space from the neural network is always trained such that major cluster heads to zero to ensure its mean, whereas a minor cluster heads to the other extreme, that is, unity, to satisfy its variance so that the proposed architecture enhances the sensitivity separating two clusters. Therefore, the proposed neural network in this study is effective at solving the issue of unsupervised anomaly detection, which features a highly imbalanced data distribution. Especially, the acquired latent space can be used as an excellent evaluation space for fault detection and prediction of the system of interest because of the repeatability and sensitivity of the proposed neural network architecture.

C. MMH METHOD

This phase consists of three major steps. The first step is to acquire a latent space where the distance between two clusters representing normal and fault conditions is maximized through Bayesian optimization for various high-level feature extractors. This process was only conducted to obtain available hyperparameters for VAEs because the distances are always set as the maximum, that is, $\sqrt{2}$, in the constrained latent space as long as the models converge and the acquired latent space is specially called MMH hereafter. Note that there is a basic assumption on the given situation: there must be at least one abnormal data. Otherwise, operational conditions within the normal cluster would be separated into both extremes because the proposed method separates two imbalanced clusters as long as any characteristic differences between those clusters exist. Therefore, the base assumption of the proposed method is that there are faulty and normal data comprising minor and major clusters similar to most real-world problems.

First, the distance was calculated based on two SVM marginal boundaries that cross the support vectors of normal and faulty clusters and was maximized. The hyperpara-meters of the VAE were delicately calibrated in this step. Otherwise, the VAE could diverge under improper hyperparameters, resulting in the maximum distance between the two clusters not being achieved with unreasonable hyperparameters. Bayesian optimization, which is most widely used, was used for this process among many optimization methods. This method is effective for hyperparameter optimization because it can solve a nonconvex problem with relatively few evaluations [51]. Tree-structured parzen estimator approach (TPE) was applied for modeling prior distributions [51]. Specifically, this study selected the distance between two clusters, normal and faulty, as an object value to be maximized because the distance is a metric that indicates the sensitivity of RUL dividing clusters of normal and fault.

Strictly speaking, therefore, the proposed method is a hybrid method featuring both supervised and unsupervised methods because the MMH itself does not require any label when the model is trained, whereas a few labels are limitedly required when hyperparameters are optimized to calculate the distance. Specifically, a distance between normal and faulty cannot be calculated in the situation when any label is unavailable in the conventional architecture of the AE considering the characteristic of unsupervised learning, i.e.,

sparse and random distribution of clusters throughout the latent space. By contrast, the proposed method can easily calculate the distance between major and minor clusters with only one labeled point from major and minor clusters in that two clusters are densely distributed at each extreme of the latent space. Note that this feature would be originated from the characteristic of supervised learning. This would be the main reason that the proposed method is a hybrid method, outperforming other architectures of AE for fault detection and failure prediction.

Next, the acquired MMH was used for two purposes in prognostics and health management (PHM). One is fault detection in a binary form of normal and fault, and the other is fault prediction, that is, estimating the RUL in a decimal form from the normal condition (defined as 1) to fault (defined as 0) by addressing a distance-based RUL estimator method, which is newly proposed in this study. Specifically, two clusters separated by the MMH can be used for anomaly detection. This study addresses the SVM as a classifier because it is simple, accurate, and robust [52]. Specifically, SVM aims to find an optimal separating hyperplane (OSH) that divides two clusters with maximum margins from edge points, which are called support vectors [53]. Suppose the binary classification datasets with N cases in the latent space as $\{\mathrm{x}_i, y_i\}$ $(1 \leq i \leq N, y_i \in \{-1, +1\})$. The linear OSH is described as

$$\mathbf{w}^{\mathbf{T}}\mathrm{x}_i - b = 0, \tag{1}$$

where $\mathbf{w}$ and b denote weight and bias, respectively. From a fault detection perspective, applying linear SVM to MMH is effective because the boundary between normal and faulty conditions is distinct such that the two different conditions can be classified with a single line.

Then, a distance-based RUL estimator was developed using MMH for fault prediction. This method utilizes the distance between two support vectors from an SVM for calculating RUL of each state. The equation of boundaries can be described in summation form as

$$x_{upper,k} = \frac{-\sum_{n=1}^{k-1} w_n x_{upper,n} - \sum_{n=k+1}^{H} w_n x_{upper,n} + b + 1}{w_k}, \tag{2}$$

and

$$x_{lower,k} = \frac{-\sum_{n=1}^{k-1} w_n x_{lower,n} - \sum_{n=k+1}^{H} w_n x_{lower,n} + b - 1}{w_k}, \tag{3}$$

at a given axis k, where k denotes any axis of the latent space because orthographic distances can be substituted for Euclidean distances when calculating the ratio between two distances. The boundaries on each side can be normal or faulty depending on the location of the normal and faulty clusters. However, the lower bound was assumed to be a normal condition boundary, whereas the upper bound was a faulty condition boundary because the major and minor clusters always head to the lower and upper boundaries, which is attributed to the characteristics of the VAE. The equally divided space between the two boundaries can be used to estimate the RUL in decimal numbers as

$$\sum_{n=1}^{H} w_n x_{i,n} = b', b - 1 \leq b' \leq b + 1, \tag{4}$$

and

$$RUL = \frac{\frac{b'}{w_k} - x_{Upper,k}}{x_{lower,k} - x_{Upper,k}} \tag{5}$$

where b' denotes the intersection of the line at axis k, which passes the given point and is parallel to the decision boundaries. The maximum and minimum RUL were set to be 1 and 0, respectively, at the borderline passing through support vectors at the normal cluster (at $b' = b - 1$) and the faulty cluster (at $b' = b + 1$). The lower and upper regions of the decision boundaries of the normal and faulty clusters were assumed to have RUL values of 1 and 0, respectively. Therefore, the proposed method quantitatively estimates the health of an elevator door.

III. EXPERIMENT

A. DATA ACQUISITION

Operational data on elevator doors were collected from an elevator located in an apartment in Seoul, Republic of Korea, which was randomly selected. The exact location of this test bench is confidential for personal information issues regarding residents living in apartments and nondisclosure agreements with the elevator operation and maintenance company. The operating conditions or physical properties of the elevator were not special. That is, they are practically the same as those of normal elevators installed at any place in Korea and other regions. Therefore, these measurements demonstrate the effectiveness of the proposed method in real-world applications. The data were recorded for 30 days from April 1, 2020, to April 30, 2020, and the total length of the data was 18,603,367.

Measurements comprise 17 different pieces of information related to the control of an elevator door, which contains both real- and Boolean-type data, as listed in Table 1. Seven real-number-type datasets include the current time, floor, door position, door speed (reference and feedback), and torque (reference and feedback) at each measurement period. In contrast, 10 Boolean-type data represent order and safety signals, including door opening, door closing, multi-beam, safety beam, close limit, open limit, close command, open command, hatch door limit, and gate door limit. Because elevator doors are controlled by embedded microprocessors without any data acquisition unit (DAQ) or data storage, monitoring their health is challenging. This configuration limits the analysis of the faulty conditions of elevator doors in previous studies. In contrast, the operation and maintenance company installed a DAQ for data acquisition at the selected elevator of interest to study the prognostic method in this study whereas any other additional sensors were not installed as normally

did in other studies [54]. Therefore, the measurements effectively show that the proposed method would be effective in real-world operations.

TABLE 1. Description of raw data collected from the elevator.

Data name	Data type	Data description	Range	Unit
Time	Real-number data	Year, Month, Date, Hour, Minute, Second	—	—
Floor		Floor of the elevator	(2–31)	floor
Door position		Location of the door	(295–840)	mm
Reference speed	Real-number data	Reference speed for a door motor	(0–60)	RPM / 5
Feedback speed		Feedback speed for a door motor	(0–60)	RPM / 5
Reference torque		Reference torque for a door motor	(0–40)	A
Feedback torque		Feedback torque for a door motor	(0–40)	A
Door close	Boolean-type signal	Door close: 1 Otherwise: 0	(0,1)	—
Door open		Door open: 1 Otherwise: 0	(0,1)	—
Multi beam		Door interrupted: 1 Otherwise: 0	(0,1)	—
Safety edge		Safety edge touched: 1 Otherwise: 0	(0,1)	—
Close limit		Close limit: 1 Otherwise: 0	(0,1)	—
Open limit		Open limit: 1 Otherwise: 0	(0,1)	—
Close command		Close command: 1 Otherwise: 0	(0,1)	—
Open command		Open command: 1 Otherwise: 0	(0,1)	—
Hatch door limit		Hatch door close state: 1 Otherwise: 0	(0,1)	—
Gate door limit		Gate door close state: 1 Otherwise: 0	(0,1)	—

B. DATASET DESCRIPTION

This section describes the dataset in detail. The refined strokes after preprocessing were classified into each health condition by an expert system, resulting in the ground truth when estimating the accuracy of the proposed method. Table 2 lists the number of strokes classified by an expert system comprising complete and incomplete strokes for both open and close strokes. Note that the small difference between the number of open and close strokes exists because strokes collected from outside of the predefined frequency were eliminated. Specifically, the strokes were defined as complete strokes when completely opened and closed states were followed by the opposite states. In contrast, partially closed and re-open strokes were defined as incomplete strokes because of the interruption by command of a customer or physical interruption in the middle of a closing stroke. This discrimination of strokes can be easily conducted because the same type of limit signal is activated after the signal turns off in this situation. The total number of strokes is 23933 and 23928 for open and close strokes, respectively, including the number of incomplete strokes for 1260 and 1251. Incomplete strokes were excluded from the target of fault detection and prediction in this study because they were inappropriate for determining the health condition of door motors. This decision can be explained by the fact that the delay effect is challenging to find in incomplete strokes, suggesting that judging the health condition of each incomplete stroke is inefficient and inaccurate even for experts. Therefore, this study focuses on fault detection and prediction based on complete strokes, not only to secure high accuracy and robustness but also to improve efficiency for embedding real-world applications. As a result, complete strokes were classified into three conditions: normal, degradation, and faulty based on the system of elevators analyzing Boolean signals and physical properties. Only normal and faulty conditions existed during close strokes, whereas normal, degradation, and faulty conditions existed during open strokes. The detailed physical origin of this different classification for open and close strokes is described in Section IV. A.

TABLE 2. Distribution of the dataset based on the health of door motors for open and close states.

Stroke type	Complete strokes			Incomplete strokes	Total number of strokes
	Normal	Degradation	Faulty		
Open	22605	32	36	1260	23933
Close	22646	0	31	1251	23928

Next, three types of statistical features were extracted from seven types of physical properties, resulting in 21 types of features as listed in Table 3. Specifically, the statistical features include peak, mean, and RMS and the seven measurements included door location, reference speed, feedback speed, differential speed, reference torque, feedback torque, and differential torque whereas the measurements irrelevant to door status such as time, floor and Boolean-type safety signals were excluded.

C. MODEL CONSTRUCTION

This section illustrates the model construction process in detail. Figure 2 shows the architecture of the VAE constructed in this study, which follows a simple VAE comprising four layers for the encoder and decoder. Twenty-one features were used as inputs, and the data were compressed into dimensions with sixteen, eight, four, and two. The last layer of the encoder consists of two nodes for means and two nodes for standard deviations. Basically, the architecture of the encoder and decoder (e.g., number of layers, number of nodes at each layer) must be optimized with other hyperparameters through

TABLE 3. List of 21 features used for the training and testing.

Feature number	Feature name
1-3	Door location (Peak, mean, RMS)
4-6	Reference speed (Peak, mean, RMS)
7-9	Feedback speed (Peak, mean, RMS)
10-12	Differential speed (Peak, mean, RMS)
13-15	Reference torque (Peak, mean, RMS)
16-18	Feedback torque (Peak, mean, RMS)
19-21	Differential torque (Peak, mean, RMS)

the hyperparameter optimization process. In this study, however, the architecture was optimized only with a rule of thumb for two reasons. One is that the architecture already showed perfect accuracy for fault classification as shown in Table 7 and our main concern in this paper is the coherence of each cluster in latent space, the phenomenon which is already shown in Figure 8. The other is that there are constraints for the design of the encoder and decoder that an encoder must compress a higher dimension to a lower one, and the opposite for a decoder: these constraints must be applied to an optimizer and those conditions might be obstacles to finding an accurate solution.

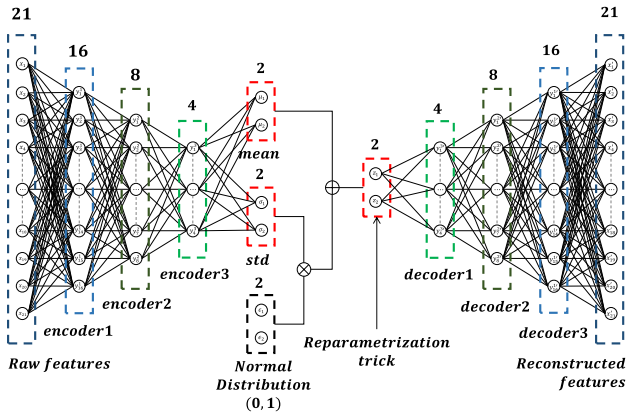

FIGURE 2. Architecture of VAE proposed in this study for diagnostic and prognostic purposes.

Therefore, other hyperparameters including activation functions of encoder and decoder, batch size, normalization type, epoch, and learning rate were optimized with the Bayesian optimizer described in Section II-C. Note that models for open and close strokes were separately optimized and the optimized hyperparameters are shown in Table 4. Hyperparameters of other models used for comparative studies were also optimized through Bayesian optimization for fair comparison and optimized hyperparameters for other models are shown in Appendix B (as shown in the supplementary material published on ieeexplore.ieee.org). SVM also has hyperparameters including C and gamma parameters but default setting (i.e., 100 and 0.01 for C and gamma value, and linear kernel) was used because the objective of the study is to focus on the effect of feature extraction, and SVMs are just utilized for classifier.

TABLE 4. Optimized hyperparameters of VAE with restricted latent space for achieving MMH.

Stroke type	Open	Close
activation function of the encoder layer	tanh	tanh
activation function of the decoder layer	tanh	tanh
batch size	1024	392
normalization type	min-max, [-1,1]	min-max, [-1,1]
epochs	1336	2432
learning rate	5.34e-3	5.88e-3
optimizer	adam	adam

D. EVALUATION METRICS

This section describes the evaluation metrics for testing. First, K-fold cross-validation was used for testing the proposed method because only a small number of strokes were available in the faulty condition. The entire dataset was divided into five small datasets, and all datasets were set to be equally distributed because scarce data could be easily concentrated in a certain dataset. All datasets except one were used for training, and the rest were used for testing so that data imbalance could be compensated. The prediction result is listed in the shape of a confusion matrix as shown in Figure 3.

		Predicted	
		Positive	Negative
Actual	Positive	True positive (TP)	False negative (FN)
	Negative	False positive (FP)	True negative (TN)

FIGURE 3. Confusion matrix.

Indexes for classification could be divided into accuracy, precision, recall, and F1 score. The accuracy is the fraction of correct predicted data from the entire dataset and could be calculated by dividing true positive (TP) and true negative (TN) by the sum of TP, TN, false positive (FP), and false negative (FN) as

$$Accuracy = \frac{TP + TN}{TP + TN + FP + FN}. \quad (6)$$

Negative predictive value (NPV) is the fraction of true negative data from the entire number predicted as negative and

could be calculated by dividing the number of TN data by the sum of TN and FN as

$$NPV = \frac{TN}{TN + FN}, \tag{7}$$

and a higher value denotes high accuracy. Precision is the fraction of true positive data from actual positive data and could be calculated by dividing TP data by the sum of TP and FN as

$$Precision = \frac{TP}{TP + FP}, \tag{8}$$

whereas recall is the fraction of true positive data from actual positive data and could be calculated by dividing TP data by the sum of TP and FN as

$$Recall = \frac{TP}{TP + FN}. \tag{9}$$

The F1 score, which is the harmonic mean of precision and recall as

$$F1score = \frac{2 \times Precision \times Recall}{Precision + Recall}, \tag{10}$$

and it was used as a metric for performance evaluation because it is widely used to verify the accuracy of neural networks on unbalanced datasets [55]. Therefore, the F1 score is the metric ranging from 0.0 to 1.0, where a higher F1 score denotes high accuracy. Three iterations were executed to estimate the F1 scores, and the mean of these scores was used as the evaluation metric.

IV. RESULT AND DISCUSSION

This section presents an in-depth discussion of the physical characteristics of door faults and the effectiveness of the MMH method. The physical characteristics of measurements depending on the different types of health conditions are explained in Section A. The dependency of stroke time on health conditions is discussed in Section B. The strengths of the proposed method are quantitatively noted in Section C, comparing different types of high-level feature extractors. Finally, the effectiveness of the method for real-world applications is validated in section D.

A. MEASUREMENT CHARACTERISTICS OF STROKES AT THREE DIFFERENT HEALTH CONDITIONS

This subsection describes the unique characteristics of open and close strokes when an elevator door motor degrades over time resulting in a faulty stroke. The strokes representing each health condition were selected from the dataset for this demonstration, whose health conditions were labeled by an expert system. Other strokes show similar behaviors and patterns so those are omitted herein for the sake of brevity.

Figure 4(a) to (c) show the entire behavior of the measurements, including the open command signal, door position, rotating speed, and torque (reference and feedback) for the normal, degradation, and faulty strokes of an elevator door at open strokes. In normal conditions (Figure 4(a)), the reference speed rises first when the open command is turned on, and the feedback speed directly follows the reference speed. The corresponding reference and feedback torque simultaneously change, resulting in a door position from 295 mm to 840 mm. The door positions of 295 mm to 840 mm denote completely closed and opened states, respectively. Therefore, the gaps between the reference and feedback for torques and speeds were small. Different trends were observed in speed and torque profiles when an elevator door suffered degradation (Figure 4(b)). A significant time delay of over three sec occurs between the measured reference and feedback speed. This observation might have occurred because the feedback speed could not follow the reference speed for the first three sec. This difference between the reference and feedback speed results in the rise of the torque. The reference torque rises to the maximum to follow the reference speed, also resulting in the feedback torque increasing to the maximum because the door does not open in the first three sec. The maximum torque imposed on the motor of an elevator door during this period might accelerate the degradation of the motor because a significant overload was imposed during this period. The speed and torque behaviors are significantly different when a fault occurs at the elevator door (Figure 4(c)). Faulty strokes follow degradation strokes in time-series data, confirming that overload imposed during a degradation period might result in the fault of the elevator door. During the early stages of a faulty stroke, the door behaves similarly to the normal condition. However, it does not completely open, making the door open very slowly at the end. Therefore, the door position moved from 295 mm to 835 mm, which was not a completely opened state, implying that an elevator could not operate in this state because of safety concerns. Moreover, the reference and feedback torque remained at the maximum values when a difference between the reference and feedback speeds existed after three sec, resulting in the door motor continuously remaining under extreme load conditions. This extreme load condition might trigger a severe failure of the door motor, which requires immediate inspection.

Figure 5 (a) and (b) represent the entire behavior of the same measurements at a close stroke for normal and faulty conditions. A close signal, which was a state signal, was used as a reference with a close command signal to divide each stroke in that the close command was still activated even after a door was already closed for safety reasons, whereas the close signal was directly turned off as soon as the door was closed. Therefore, dividing each stroke by employing both command and state signals is an effective way to chop into each stroke. In normal conditions (Figure 5 (a)), the reference speed increases first, and the feedback speed directly follows the reference speed. The reference and feedback torque varied to close a door, resulting in a door position moving from 840 mm to 295 mm, representing completely opened and closed states. Unlike a normal stroke in an open stroke, torque was applied for a short time when a normal stroke started in a close stroke. This observation can be attributed to the fact that closing doors are frequently interrupted by

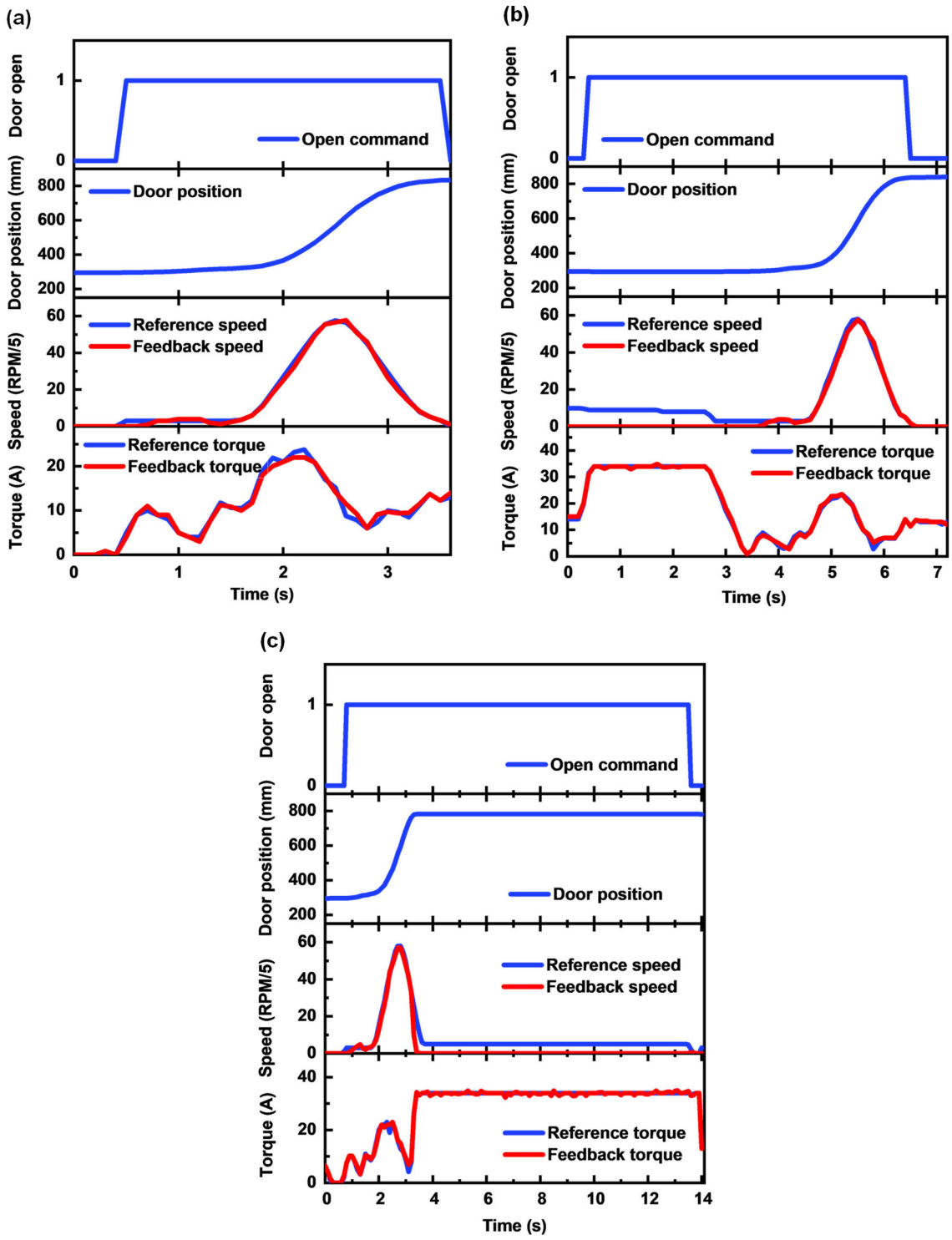

FIGURE 4. Four types of physical characteristics including open command signal, door position, speed, and torque for each health state of a door motor in open state. Each subfigure denotes (a) normal, (b) degradation, and (c) faulty conditions.

passengers or obstacles so closing the door with high speed and torque is unsafe, which may result in severe damage to both passengers and door systems. The remaining inertia after applying a small torque at the beginning results in the door closing. The feedback speed cannot follow the reference speed under faulty conditions (Figure 5 (b)), causing the reference and feedback torque to be maximized to compensate for the gap between the reference and feedback speed. After the door barely starts to move, the torque drops rapidly for safety, and the door slowly closes because it lacks inertia

compared to that in normal conditions, requiring more time to be closed.

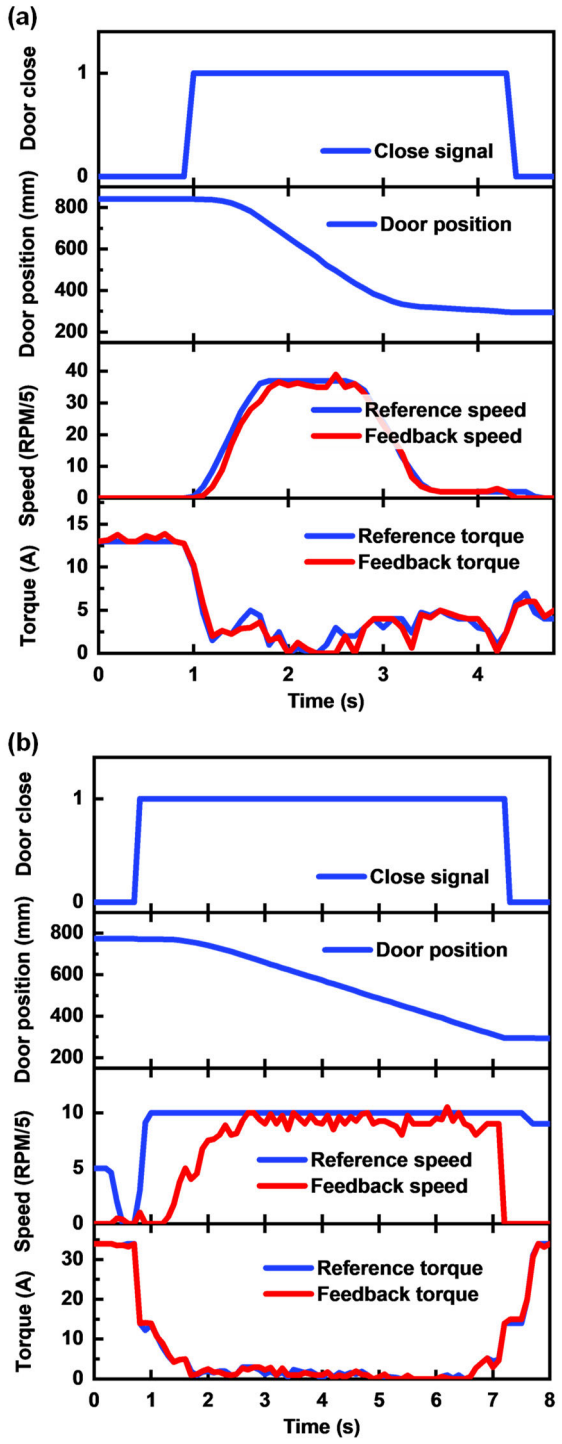

FIGURE 5. Four types of physical characteristics including close signal, door position, speed, and torque for each health state of door motor in close state. Each subfigure denotes (a) normal, and (b) faulty conditions. The main difference between those of open state is that there is no degradation state at a close stroke.

In summary, conventional symptoms of faulty conditions for both open and close strokes could be characterized by analyzing the gap between reference and feedback speeds, excessive torques, and slow rotating speed of motors overall. Additionally, the main difference between open and close strokes is that no degradation strokes exist when the elevator door is closing. Only normal and faulty conditions exist in close strokes. Health condition is less clearly indicated for close strokes compared to that of open strokes because torque is applied only for a short period when starting each stroke to provide inertia so that the health condition of the motor is blurred. Therefore, this study only used measurements of open strokes to monitor the health condition of the elevator doors effectively.

B. DEPENDENCY OF OPERATIONAL TIME ON THE HEALTH CONDITION OF THE ELEVATOR DOOR

The analysis of the speed and torque behaviors of the elevator door revealed that these measurements significantly depend on the health condition of the elevator door. This physical correlation suggests that the operational time might depend on the health condition of each stroke. Therefore, the total operational time of each stroke was analyzed for in-depth discussions of the fault analysis of an elevator door. The controller of the elevator door does not measure the total operational time of each stroke. This study independently calculated the operational time of each stroke by analyzing various digital signals. Figure 6 illustrates the distribution of the total operational time for open and close strokes. The vertical and horizontal axes denote the number of strokes on a log scale and the total operational time for each stroke, respectively. The three different colors in each column indicate health conditions classified as normal, degradation, and faulty.

The analysis of the total operational time at the open stroke shows that the three strokes are clearly classified into three clusters (Figure 6 (a)). A normal condition was represented by 22605 strokes distributed between 3.2 s and 4.1 s. This distribution indicated that a period of 3 s to 4 s was required to open an elevator door under normal health conditions. Second, 32 strokes were distributed from 6.6 s to 7.1 s, representing the degradation condition. The delay might occur at an early phase of the strokes, as mentioned in section IV-A, resulting in a discrepancy of a few seconds under a degradation condition. Third, 36 strokes ranged from 13.9 s to 14.7 s, all of which were judged as faulty strokes. The total operational time for faulty strokes is four times longer than that for normal strokes. Faults occurring at motors resulted in a longer period of total operational time after a small delay occurred during the degradation period under extreme load conditions. Therefore, the total operational time for each stroke could become a sensitive metric representing a health index to detect anomalies in an elevator door because this metric clearly separated normal, degradation, and faulty clusters.

In contrast, strokes were divided into two clusters in close strokes (Figure 6 (b)). Specifically, 22646 strokes were distributed from 3.2 s to 4.4 s, suggesting that the time was

consumed in the normal condition at the close strokes. Additionally, 31 strokes ranged from 7.2 s to 7.7 s, all of which were judged to be faulty strokes. The physical characteristics of open and close strokes suggested that the door opens by imposing huge motor torque during the entire period of the open stroke, whereas the motor applied a small amount of torque in a short period, and the door operated with inertia in the rest of the period at the close stroke. Therefore, the motor health condition would be less correlated with measurements of control information in the period of inertia operation at the close stroke because torque from the motor was not required in this period. The difference in operational principles between open and close strokes results in the degradation condition appearing only in the open stroke because the open stroke is highly correlated with the control method of the motor, suggesting that the open stroke is essentially more sensitive to the motor health condition. However, the total operational time for each stroke at the close strokes can be used for fault detection because a sufficient gap is secured between the two clusters of each health condition.

In summary, measurements of operational information at the open stroke can be used for fault detection and prediction, whereas those at the close stroke can be used only for fault detection.

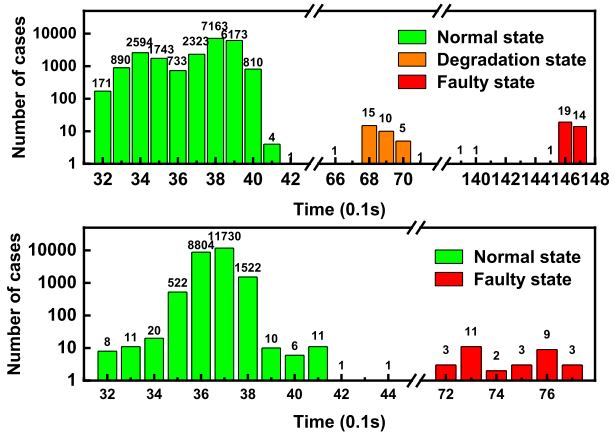

FIGURE 6. Distribution of the total operational time at each health condition for open and close strokes. Subfigure (a) and (b) represent the distribution of strokes at open and close state. Green, orange, and red bars each denote the number of strokes at normal, degradation, and faulty health state.

C. MMH ACQUIREMENT

This subsection describes the procedure for acquiring MMH and the effectiveness of the VAE for separating major and minor clusters by quantitatively comparing the performances of the VAE and AE. The hyperparameters of the AE and VAE were optimized through Bayesian optimization by setting a marginal distance between the normal and faulty clusters as an objective value to be maximized for a fair comparison. The optimized hyperparameters from Bayesian optimization are listed in Appendix B (as shown in the supplementary material published on ieeexplore.ieee.org). Note that other state-of-the-art methods are excluded from the comparison because these two algorithms are accurate enough for classifying the target dataset and the main interest of the study is to apparently separate two classes in latent space.

Figure 7 shows the distance between normal and faulty clusters with different types of AE. Theoretically, the maximum distance between two clusters should be $\sqrt{2}$, which is the diagonal length of the square one on a side. The distance from the VAE was 1.4142 for both open and close strokes, whereas those from the AE were 0.9747 and 0.9979, respectively. This result suggests that the VAE could converge to the global minimum solution, whereas the AE could converge to the local minimum solution because the distance from the AE was less than the theoretical maximum value. By creating latent vectors at each latent space dimension in accordance with standard normal distributions, the VAE separated two clusters with the maximum distance. The distances between the two clusters at VAE were same regardless of stroke type, whereas distances of AE showed a difference of 2 % between open and close strokes, confirming that the robustness of the VAE is higher than that of AE. Therefore, the result confirms that VAE features high robustness in finding the global minimum solution, whereas the neural network created by AE is vulnerable to the convergence of the local minimum solution.

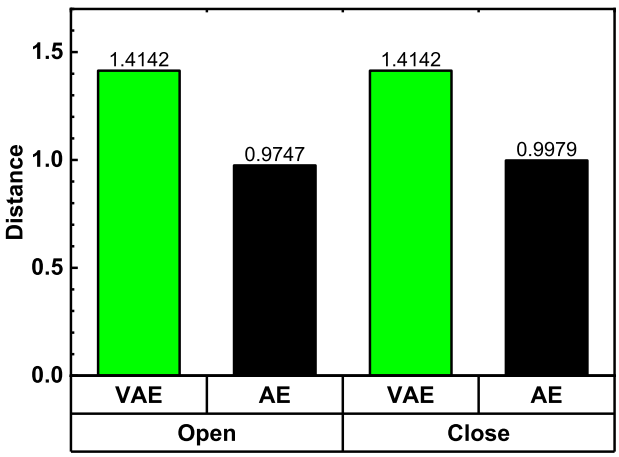

FIGURE 7. Comparison of the maximized margin distance between when using AE and VAE is represented to show the maximized sensitivity when using the proposed method.

To further emphasize the effectiveness of the VAE as a feature extractor, statistical values, including the mean and variance of each cluster, were compared. These two metrics would be good metrics for comparing the differences between VAE and AE in that the constant means and low variances in different training cases indicate the robustness of the feature extractor. Table 5 (a) shows the means and variances for an open stroke, and Table 5 (b) presents those for a close stroke. Note that the types of VAE are divided into two types again for validating the effect of regulation, a VAE regulated with sigmoid activation function and the other one which is unregulated. The statistical values were calculated in each latent dimension and both spaces are indicated as latent

TABLE 5. Statistical comparison of clusters at each latent dimension, health condition, and types of AEs for each type of stroke is represented to suggest the coherence of each cluster. Tables (a) and (b) represent those at open and close states.

(a) Open strokes

Health state	Latent dimension	VAE		VAE (w.o./ regulation)		AE	
		Mean	Variance	Mean	Variance	Mean	Variance
Normal	Dim 1	4.28×10^{-9}	3.68×10^{-24}	-0.72	10.90	0.964	1.31×10^{-4}
	Dim 2	1.91×10^{-9}	1.05×10^{-29}	2.47	35.55	0.434	6.64×10^{-3}
Faulty	Dim 1	1.0	0.0	44.53	48.23	0.397	2.19×10^{-2}
	Dim 2	1.0	0.0	30.95	183.56	0.921	9.14×10^{-4}

(b) Close Strokes

Health state	Latent dimension	VAE		VAE (w.o./ regulation)		AE	
		Mean	Variance	Mean	Variance	Mean	Variance
Normal	Dim 1	1.91×10^{-9}	1.43×10^{-25}	5.86×10^{-2}	1.61	0.964	1.31×10^{-4}
	Dim 2	2.11×10^{-9}	1.61×10^{-25}	-7.20×10^{-2}	1.28	0.434	6.64×10^{-3}
Faulty	Dim 1	1.0	0.0	-8.38	3.56×10^{-3}	0.397	2.19×10^{-2}
	Dim 2	1.0	0.0	-0.38	4.14×10^{-3}	0.921	9.14×10^{-4}

dimension 1 (Dim 1) and 2 (Dim 2). Constant means near two extremes and low variances were characterized when addressing regulated VAE in both open and close strokes, whereas random means and relatively high variances were shown for each health condition in both dimensions when addressing unregulated VAE and AE. The normal cluster occupying most of the distribution was transformed to near the origin (i.e., zero) in the latent space when the regulated VAE was used, whereas the normal clusters at the latent space of the unregulated VAE and AE were randomly distributed. In contrast, the faulty cluster containing only a few cases was transformed to the opposite extreme of unity, confirming that the regulated VAE would induce minor clusters to be located at unity in the transformed latent space. These observations confirm again that sigmoid function plays a regularization role at each latent space to maintain the means of the total distribution as zero, elucidating the effectiveness of the VAE in making decisions based on the distribution of features in the latent space because the boundaries between normal and abnormal clusters would be constant in similar cases.

In summary, VAE is effective for transforming input data with an unbalanced distribution into those at a low-dimensional latent space in that the method could effectively separate major and minor clusters with the maximum distance between them by ignoring minor differences within the clusters. Moreover, the separated clusters are concentrated at each extreme so that their classes can be easily classified without any supervision.

D. APPLICATION FOR DIAGNOSIS AND PROGNOSIS

This subsection describes the application of the MMH method for classifying strokes as normal or faulty and predicting the RUL of an elevator door. The confusion matrices for each stroke and evaluation matrices are tabulated in Table 6 and Table 7 by addressing the SVM with different types of features to elucidate the origin of the misclassified strokes. NPV will be mainly discussed in this part because other indexes showed almost perfect results because of the extreme imbalance of the dataset.

First, only 15 statistical features from the measurements were employed to classify the health status of each stroke (Table 6 (a)). All normal strokes were correctly classified as normal, whereas the three faulty strokes were misclassified as normal. The NPV for open and close strokes were 0.917 and 1.0, respectively. Additionally, six manipulated features were added to the previous dataset to demonstrate the effectiveness of feature manipulation. Two misclassifications decreased in open strokes, while one fault stroke was still misclassified as a normal condition, increasing the NPV from 0.917 to 0.972. This improvement suggests that accuracy could be enhanced with knowledge-based feature manipulation, similar to that in the literature [48], confirming that the maximum performance of machine learning methods might depend on understanding of users. The results illustrate that the health condition of an elevator door can be estimated using simple preprocessing and feature manipulation methods to raw data to some degree but sometimes the prediction can be misguided. Misclassifications might arise from the inherent vulnerability of the SVM for classifying features in a high-dimensional space because of the curse of dimensionality [56]. Third, two distinct features in two-dimensional latent space, which were extracted through the VAE and AE, were used for classification (Table 6 (c)). The classification accuracy was perfect in both cases. The results are described in a single table because the same result of perfect classification was deduced regardless of the AE type. All classifications were correct even though the number of dimensions was significantly reduced from twenty-one to two, indicating that high-level features relevant to health conditions were well compressed to features in the two-dimensional latent space in both cases

and reflected as their locations in the latent space. Finally, the reconstructed features from the VAE and AE achieved the same accuracy (Table 6 (d)). Both results were described in a single table. The perfect results in the third and fourth cases suggest that AEs play a critical role in the classification at the reconstructed space because AEs have a strong noise reduction effect in common [57]. However, low-dimensional latent space would decrease the inference time for classification, suggesting that classification in the latent space might secure the best performance in terms of both accuracy and inference time. In summary, feature manipulation increased the classification accuracy from 0.917 to 0.972 in an NPV because these additional features provided sufficient information for classification. Moreover, space transformation through VAE and AE increased the NPV from 0.972 to 1.0 because nonlinear feature transformation is effective for classification. The classification result at a close stroke always shows a perfect NPV of 1.0. However, this type of stroke is limited in predicting RUL because the close motion of an elevator door is highly correlated to inertial motion, which is limited in monitoring the degradation trend of components deployed in an elevator door.

TABLE 6. Confusion matrix of elevator door stroke classification result when using: (a) raw features, (b) raw features and manipulated features, (c) high-level features encoded by AEs, and (d) features after reconstruction.

(a) Raw features

Period	True state	Predicted state	
		Normal	Faulty
Open	Normal	22605	3
	Faulty	0	33
Close	Normal	22646	0
	Faulty	0	31

(b) Manipulated features added

Period	True state	Predicted state	
		Normal	Faulty
Open	Normal	22605	1
	Faulty	0	35
Close	Normal	22646	0
	Faulty	0	31

(c) High-level features extracted from AEs

Period	True state	Predicted state	
		Normal	Faulty
Open	Normal	22605	0
	Faulty	0	36
Close	Normal	22646	0
	Faulty	0	31

(d) Reconstructed features

Period	True state	Predicted state	
		Normal	Faulty
Open	Normal	22605	0
	Faulty	0	36
Close	Normal	22646	0
	Faulty	0	31

The data distributions on each latent space were further analyzed to demonstrate the advantage of the MMH method for predicting RUL in open strokes because only open strokes include degradation symptoms. Figure 7 describes the latent space of open strokes when addressing VAE (Figure 7 (a), (b)), and AE (Figure 7 (c), (d)). First, the distributions of a latent space consisting of strokes under normal and faulty conditions are shown in Figure 7 (a) and (c) for VAE and AE, respectively. The strokes in the normal condition are denoted by green points, whereas those in the faulty condition are denoted by red points. The blue and red lines denote the lines passing through the support vectors in normal and faulty clusters, respectively. The results illustrate that feature distributions extracted from the VAE concentrate each stroke within its cluster, which can be represented by low variances of each cluster in both latent dimensions, whereas the features extracted from an AE are widely distributed in the latent space. The clusters of the normal and faulty conditions from the VAE are located at the origin and the other extreme, which could be represented by means close to 0.0 and 1.0, whereas the features extracted from an AE are randomly located. These results suggest that the clusters from the VAE would be a more distinct metric for fault classification than those from the AE.

To highlight the effectiveness of the proposed method, the RULs at given locations are shown in Figure 8 (b) and (d) using the distances from each cluster to the locations of the state of interest, when compressed with VAE and AE. The line passing through a support vector in the normal cluster (the blue line in Figure 8) and outside of the line is defined as an RUL of 1.0, and the line passing through a support vector in the faulty cluster (the red line in Figure 8) and outside of the line is defined as an RUL of 0.0, indicating that a fault occurred at that moment. The reserved hyperspace between the two lines of the support vector is the degradation region in this configuration, and the OSH (the black line in Figure 8) is considered as a reference line, which is defined as the border between a healthy and unhealthy state representing an RUL of 0.5 because the distances from the OSH to both clusters are always the same. This assumption might be unreasonable because most degradation procedures are nonlinear; however, AE transforms nonlinear input space into linear latent space, and it rationalizes the assumption. The strokes in a degradation state denoted by orange points, which were identified from open strokes, are located in the degradation region (Figure 8 (b) and (d) for VAE and AE). This observation suggests that estimating a degradation state, that is, a healthy condition, is possible at this MMH because the MMH is well-regulated to reflect only the major difference between healthy and faulty clusters during an open stroke. In contrast, estimating a degradation state with features extracted from an AE would be inappropriate because the clusters of normal and faulty states are widely and randomly distributed, which confuses the exact decision. Furthermore, latent space distribution varies with the initial values of weights and iterations when addressing AE, which

TABLE 7. Various metrics of elevator door stroke classification result when different types of features are utilized.

Methods	Accuracy	NPV	Precision	Recall	F1 score
Raw features	0.99987	0.917	1.0	0.99987	0.99993
Manipulated features added	0.99996	0.972	1.0	0.99996	0.99998
Latent space (from AE)	1.0	1.0	1.0	1.0	1.0
Latent space (from VAE)	1.0	1.0	1.0	1.0	1.0
Reconstructed features	1.0	1.0	1.0	1.0	1.0

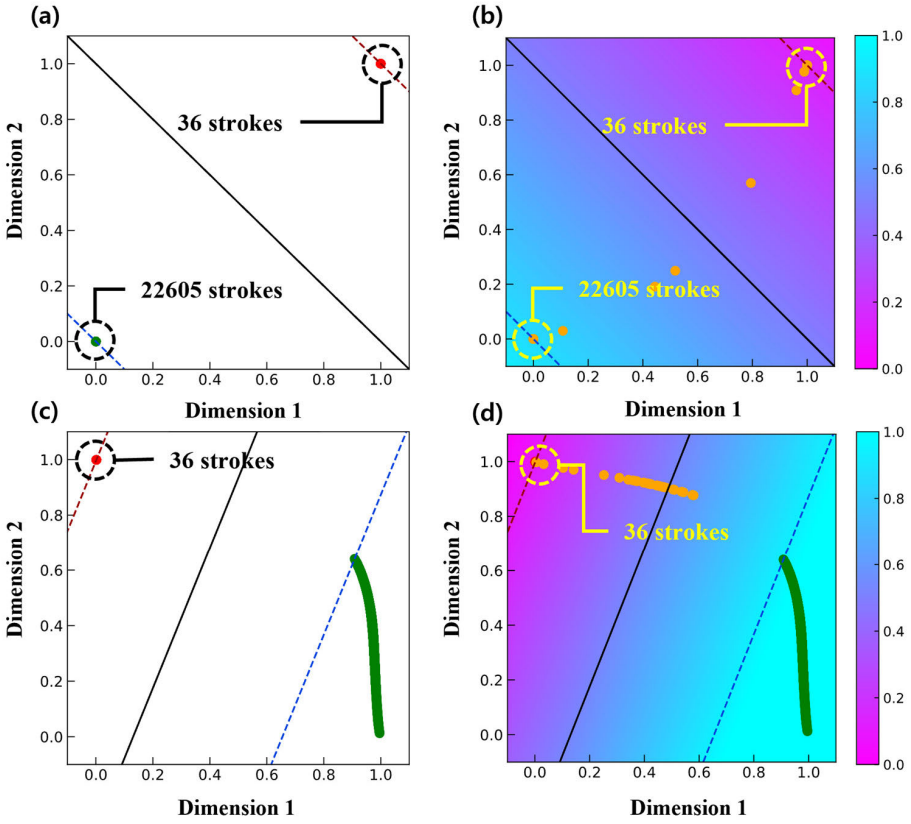

FIGURE 8. Two-dimensional latent space of open strokes extracted from different types of AE. (a) represents the distribution of each cluster on latent space encoded by VAE. (b) represents the distribution of each cluster on latent space encoded by VAE but with the colormap representing distance-based RUL estimation. (c) represents the distribution of each cluster on latent space encoded by AE. (b) represents the distribution of each cluster on latent space encoded by AE but with the colormap representing distance-based RUL estimation.

hinders operators of elevators from estimating the health states of an elevator door in real-world applications. Lastly, for validating the appropriacy of the proposed method on real-time deployment, the time consumption on each prediction by MMH method is calculated by measuring time consumption for 500 predictions and averaging them. When a door stroke occurs, statistical features are extracted from each open and close stroke, going into the model instead of using them in a time window form. The start and stop points of each stroke are defined using Boolean-type operating command signals. Specifically, open stroke is defined as the time when the open command signal turns on, whereas close stroke is between the period when the open limit turns off and the close limit signal turns on because the close command keeps turning on even after a door is completely closed for safety reasons. Note that all experiments were conducted on a desktop with two intel Xeon E5-2620 v4 (2.10 GHz) CPUs, 64 GB memory, two RTX-2080ti GPUs, and Ubuntu 18.04 with Tensorflow 2.4.1. The averaged FPS is calculated as 61.34, the same as 0.016 s per stroke. This time consumption is much shorter than that of each stroke, i.e., longer than 3.2 s, which means that the real-time application of the algorithm is available even for a generally used single-board computer. In summary, the proposed MMH could be effective in detecting faults in elevator doors because high-level features containing information about health conditions are effectively compressed into the latent space. Additionally, the method could be effective at finding potential faults that occur at the open stroke because the locations of two clusters are reserved through statistical nonlinear space transformation so that strokes in a degradation state can be easily detected without any supervision. Furthermore, the proposed method quantitatively provides

the RUL of the system of interest without defining the RUL of the system, which is a challenging task in real-world applications.

V. CONCLUSION

This study proposed an MMH, which is a sensitivity-maximized latent space for classifying normal and abnormal clusters. This method tackles the existing unsupervised classification problem with a highly imbalanced data distribution without information for the RUL, a common and challenging problem in real-world applications. Specifically, first, the knowledge-based feature manipulation provides additional information for fault classification. Subsequently, the VAE transforms the original spaces into distinct latent spaces, enabling perfect fault classification through a statistical nonlinear space transformation. Finally, the MMH is acquired by maximizing the distance from a major to a minor cluster through Bayesian optimization, which is effective for fault classification and prediction. From a diagnostic perspective, the MMH is useful for dividing dominant and sparse clusters because it shows high sensitivity and locational constancy. Additionally, the distance from each cluster in the MMH can be used to predict RUL from a prognostic perspective. The effectiveness of the proposed method was demonstrated using field measurements of elevator door strokes. The results show that the proposed method perfectly classifies the faults and effectively shows the RUL of an elevator door, in that the MMH is trained to only contain features highly correlated to health conditions. Future studies can be conducted in two ways. One is to collect more data from various elevators and verify the reliability of the proposed method. Another is to develop a real-time fault detection and prediction algorithm based on the proposed method.

REFERENCES

[1] D. Neupane and J. Seok, "Bearing fault detection and diagnosis using case western reserve university dataset with deep learning approaches: A review," *IEEE Access*, vol. 8, pp. 93155–93178, 2020, doi: 10.1109/ACCESS.2020.2990528.

[2] T. Orlowska-Kowalska, M. Wolkiewicz, P. Pietrzak, M. Skowron, P. Ewert, G. Tarchala, M. Krzysztofiak, and C. T. Kowalski, "Fault diagnosis and fault-tolerant control of PMSM drives–state of the art and future challenges," *IEEE Access*, vol. 10, pp. 59979–60024, 2022, doi: 10.1109/ACCESS.2022.3180153.

[3] S. R. Saufi, Z. A. B. Ahmad, M. S. Leong, and M. H. Lim, "Challenges and opportunities of deep learning models for machinery fault detection and diagnosis: A review," *IEEE Access*, vol. 7, pp. 122644–122662, 2019, doi: 10.1109/ACCESS.2019.2938227.

[4] W. Lang, Y. Hu, C. Gong, X. Zhang, H. Xu, and J. Deng, "Artificial intelligence-based technique for fault detection and diagnosis of EV motors: A review," *IEEE Trans. Transp. Electrific.*, vol. 8, no. 1, pp. 384–406, Mar. 2022, doi: 10.1109/TTE.2021.3110318.

[5] S. Tang, S. Yuan, and Y. Zhu, "Deep learning-based intelligent fault diagnosis methods toward rotating machinery," *IEEE Access*, vol. 8, pp. 9335–9346, 2020, doi: 10.1109/ACCESS.2019.2963092.

[6] M. Aishwarya and R. M. Brisilla, "Design and fault diagnosis of induction motor using ML-based algorithms for EV application," *IEEE Access*, vol. 11, pp. 34186–34197, 2023, doi: 10.1109/ACCESS.2023.3263588.

[7] C. E. Sunal, V. Dyo, and V. Velisavljevic, "Review of machine learning based fault detection for centrifugal pump induction motors," *IEEE Access*, vol. 10, pp. 71344–71355, 2022, doi: 10.1109/ACCESS.2022.3187718.

[8] S. M. K. Zaman and X. Liang, "An effective induction motor fault diagnosis approach using graph-based semi-supervised learning," *IEEE Access*, vol. 9, pp. 7471–7482, 2021, doi: 10.1109/ACCESS.2021.3049193.

[9] K.-Y. Oh, J.-Y. Park, J.-S. Lee, B. I. Epureanu, and J.-K. Lee, "A novel method and its field tests for monitoring and diagnosing blade health for wind turbines," *IEEE Trans. Instrum. Meas.*, vol. 64, no. 6, pp. 1726–1733, Jun. 2015, doi: 10.1109/TIM.2014.2381791.

[10] W. Tuerxun, X. Chang, G. Hongyu, J. Zhijie, and Z. Huajian, "Fault diagnosis of wind turbines based on a support vector machine optimized by the sparrow search algorithm," *IEEE Access*, vol. 9, pp. 69307–69315, 2021, doi: 10.1109/ACCESS.2021.3075547.

[11] R. Jegadeeshwaran and V. Sugumaran, "Fault diagnosis of automobile hydraulic brake system using statistical features and support vector machines," *Mech. Syst. Signal Process.*, vols. 52–53, pp. 436–446, Feb. 2015, doi: 10.1016/j.ymssp.2014.08.007.

[12] M. Mousavi, A. Chaibakhsh, A. Jamali, M. Kordestani, and M. Saif, "A new fault diagnosis approach for heavy-duty gas turbines," *IEEE/ASME Trans. Mechatronics*, vol. 27, no. 5, pp. 3339–3349, Oct. 2022, doi: 10.1109/TMECH.2021.3138834.

[13] J. Li, Y. Ying, and C. Ji, "Study on gas turbine gas-path fault diagnosis method based on quadratic entropy feature extraction," *IEEE Access*, vol. 7, pp. 89118–89127, 2019, doi: 10.1109/ACCESS.2019.2927306.

[14] Z. Li, D. Miao, and K. Feng, "Determining dynamic thresholds for gas turbine engine condition monitoring," *IEEE Access*, vol. 10, pp. 87404–87414, 2022, doi: 10.1109/ACCESS.2022.3198983.

[15] K. Yan, Z. Ji, H. Lu, J. Huang, W. Shen, and Y. Xue, "Fast and accurate classification of time series data using extended ELM: Application in fault diagnosis of air handling units," *IEEE Trans. Syst., Man, Cybern. Syst.*, vol. 49, no. 7, pp. 1349–1356, Jul. 2019, doi: 10.1109/TSMC.2017.2691774.

[16] K. Yan, J. Huang, W. Shen, and Z. Ji, "Unsupervised learning for fault detection and diagnosis of air handling units," *Energy Buildings*, vol. 210, Mar. 2020, Art. no. 109689, doi: 10.1016/j.enbuild.2019.109689.

[17] H. Zhang, S. Seal, D. Wu, F. Bouffard, and B. Boulet, "Building energy management with reinforcement learning and model predictive control: A survey," *IEEE Access*, vol. 10, pp. 27853–27862, 2022, doi: 10.1109/ACCESS.2022.3156581.

[18] A. Gálvez, D. Galar, and D. Seneviratne, "A hybrid model-based approach on prognostics for railway HVAC," *IEEE Access*, vol. 10, pp. 108117–108127, 2022, doi: 10.1109/ACCESS.2022.3211258.

[19] M. Achouch, M. Dimitrova, K. Ziane, S. S. Karganroudi, R. Dhouib, H. Ibrahim, and M. Adda, "On predictive maintenance in industry 4.0: Overview, models, and challenges," *Appl. Sci.*, vol. 12, no. 16, p. 8081, Aug. 2022, doi: 10.3390/app12168081.

[20] Y. Zhao, T. Li, X. Zhang, and C. Zhang, "Artificial intelligence-based fault detection and diagnosis methods for building energy systems: Advantages, challenges and the future," *Renew. Sustain. Energy Rev.*, vol. 109, pp. 85–101, Jul. 2019, doi: 10.1016/j.rser.2019.04.021.

[21] R. Ghimire, C. Zhang, and K. R. Pattipati, "A rough set-theory-based fault-diagnosis method for an electric power-steering system," *IEEE/ASME Trans. Mechatronics*, vol. 23, no. 5, pp. 2042–2053, Oct. 2018, doi: 10.1109/TMECH.2018.2863119.

[22] J. Wang, Y. Li, R. X. Gao, and F. Zhang, "Hybrid physics-based and data-driven models for smart manufacturing: Modelling, simulation, and explainability," *J. Manuf. Syst.*, vol. 63, pp. 381–391, Apr. 2022, doi: 10.1016/j.jmsy.2022.04.004.

[23] Y. Wilhelm, P. Reimann, W. Gauchel, and B. Mitschang, "Overview on hybrid approaches to fault detection and diagnosis: Combining data-driven, physics-based and knowledge-based models," *Proc. CIRP*, vol. 99, pp. 278–283, May 2021, doi: 10.1016/j.procir.2021.03.041.

[24] T. Sutharssan, S. Stoyanov, C. Bailey, and C. Yin, "Prognostic and health management for engineering systems: A review of the data-driven approach and algorithms," *J. Eng.*, vol. 2015, no. 7, pp. 215–222, Jul. 2015, doi: 10.1049/joe.2014.0303.

[25] X. Dai and Z. Gao, "From model, signal to knowledge: A data-driven perspective of fault detection and diagnosis," *IEEE Trans. Ind. Informat.*, vol. 9, no. 4, pp. 2226–2238, Nov. 2013, doi: 10.1109/TII.2013.2243743.

[26] S. Omar, A. Ngadi, and H. H. Jebur, "Machine learning techniques for anomaly detection: An overview," *Int. J. Comput. Appl.*, vol. 79, no. 2, pp. 33–41, Oct. 2013.

[27] D. Spathis, I. Perez-Pozuelo, L. Marques-Fernandez, and C. Mascolo, "Breaking away from labels: The promise of self-supervised machine learning in intelligent health," *Patterns*, vol. 3, no. 2, Feb. 2022, Art. no. 100410, doi: 10.1016/j.patter.2021.100410.

[28] A. Theissler, J. Pérez-Velázquez, M. Kettelgerdes, and G. Elger, "Predictive maintenance enabled by machine learning: Use cases and challenges in the automotive industry," *Rel. Eng. Syst. Saf.*, vol. 215, Nov. 2021, Art. no. 107864, doi: 10.1016/j.ress.2021.107864.

[29] D. E. Rumelhart, G. E. Hinton, and R. J. Williams, "Learning representations by back-propagating errors," *Nature*, vol. 323, no. 6088, pp. 533–536, Oct. 1986, doi: 10.1038/323533a0.

[30] Y. Wang, H. Yao, and S. Zhao, "Auto-encoder based dimensionality reduction," *Neurocomputing*, vol. 184, pp. 232–242, Apr. 2016, doi: 10.1016/j.neucom.2015.08.104.

[31] M. Sakurada and T. Yairi, "Anomaly detection using autoencoders with nonlinear dimensionality reduction," in *Proc. MLSDA 2nd Workshop Mach. Learn. Sensory Data Anal.*, 2014. p. 4, doi: 10.1145/2689746.2689747.

[32] D. P. Kingma and M. Welling, "Auto-encoding variational Bayes," vol. 1312, no. 6114, Dec. 2013, *arXiv:1312.6114*, doi: 10.48550/arXiv.1312.6114.

[33] J. Zhang, Y. Xu, H. Chen, and L. Xing, "A novel building heat pump system semi-supervised fault detection and diagnosis method under small and imbalanced data," *Eng. Appl. Artif. Intell.*, vol. 123, Aug. 2023, Art. no. 106316, doi: 10.1016/j.engappai.2023.106316.

[34] G. San Martin and E. L. Droguett, "Temporal variational auto-encoders for semi-supervised remaining useful life and fault diagnosis," *IEEE Access*, vol. 10, pp. 55112–55125, 2022, doi: 10.1109/ACCESS.2022.3174860.

[35] L. Zhang, H. Zhang, and G. Cai, "The multiclass fault diagnosis of wind turbine bearing based on multisource signal fusion and deep learning generative model," *IEEE Trans. Instrum. Meas.*, vol. 71, pp. 1–12, 2022, doi: 10.1109/TIM.2022.3178483.

[36] Z. Pei, H. Jiang, X. Li, J. Zhang, and S. Liu, "Data augmentation for rolling bearing fault diagnosis using an enhanced few-shot Wasserstein auto-encoder with meta-learning," *Meas. Sci. Technol.*, vol. 32, no. 8, May 2021, Art. no. 084007, doi: 10.1088/1361-6501/abe5e3.

[37] W. Khan, M. Haroon, A. N. Khan, M. K. Hasan, A. Khan, U. A. Mokhtar, and S. Islam, "DVAEGMM: Dual variational autoencoder with Gaussian mixture model for anomaly detection on attributed networks," *IEEE Access*, vol. 10, pp. 91160–91176, 2022, doi: 10.1109/ACCESS.2022.3201332.

[38] U. Yokkampon, A. Mowshowitz, S. Chumkamon, and E. Hayashi, "Robust unsupervised anomaly detection with variational autoencoder in multivariate time series data," *IEEE Access*, vol. 10, pp. 57835–57849, 2022, doi: 10.1109/ACCESS.2022.3178592.

[39] M. Shimizu, S. Perinpanayagam, and B. Namoano, "A real-time fault detection framework based on unsupervised deep learning for prognostics and health management of railway assets," *IEEE Access*, vol. 10, pp. 96442–96458, 2022, doi: 10.1109/ACCESS.2022.3205352.

[40] A. Pollastro, G. Testa, A. Bilotta, and R. Prevete, "Semi-supervised detection of structural damage using variational autoencoder and a one-class support vector machine," *IEEE Access*, vol. 11, pp. 67098–67112, 2023, doi: 10.1109/ACCESS.2023.3291674.

[41] C. Huang, Y. Chai, Z. Zhu, B. Liu, and Q. Tang, "A novel distributed fault detection approach based on the variational autoencoder model," *ACS Omega*, vol. 7, no. 3, pp. 2996–3006, Jan. 2022, doi: 10.1021/acsomega.1c06033.

[42] Z. Pan, Y. Wang, Y. Cao, and W. Gui, "VAE-based interpretable latent variable model for process monitoring," *IEEE Trans. Neural Netw. Learn. Syst.*, early access, Jun. 13, 2023, doi: 10.1109/TNNLS.2023.3282047.

[43] P. Indyk and R. Motwani, "Approximate nearest neighbors: Towards removing the curse of dimensionality," in *Proc. 30th Annu. ACM Symp. Theory Comput.*, 1998, pp. 604–613.

[44] J. Zhang, Y. Jiang, X. Li, H. Luo, S. Yin, and O. Kaynak, "Remaining useful life prediction of lithium-ion battery with adaptive noise estimation and capacity regeneration detection," *IEEE/ASME Trans. Mechatronics*, vol. 28, no. 2, pp. 632–643, Apr. 2023, doi: 10.1109/TMECH.2022.3202642.

[45] J. Zhang, C. Huang, M.-Y. Chow, X. Li, J. Tian, H. Luo, and S. Yin, "A data-model interactive remaining useful life prediction approach of lithium-ion batteries based on PF-BiGRU-TSAM," *IEEE Trans. Ind. Informat.*, early access, Apr. 11, 2023, doi: 10.1109/TII.2023.3266403.

[46] R. Jiao, X. Huang, X. Ma, L. Han, and W. Tian, "A model combining stacked auto encoder and back propagation algorithm for short-term wind power forecasting," *IEEE Access*, vol. 6, pp. 17851–17858, 2018, doi: 10.1109/ACCESS.2018.2818108.

[47] A. A. Amin and K. M. Hasan, "A review of fault tolerant control systems: Advancements and applications," *Measurement*, vol. 143, pp. 58–68, Sep. 2019, doi: 10.1016/j.measurement.2019.04.083.

[48] S. Son and K.-Y. Oh, "Integrated framework for estimating remaining useful lifetime through a deep neural network," *Appl. Soft Comput.*, vol. 122, Jun. 2022, Art. no. 108879, doi: 10.1016/j.asoc.2022.108879.

[49] L. Huang, J. Qin, Y. Zhou, F. Zhu, L. Liu, and L. Shao, "Normalization techniques in training DNNs: Methodology, analysis and application," *IEEE Trans. Pattern Anal. Mach. Intell.*, vol. 45, no. 8, pp. 10173–10196, Aug. 2023, doi: 10.1109/TPAMI.2023.3250241.

[50] G. P. Way, M. Zietz, V. Rubinetti, D. S. Himmelstein, and C. S. Greene, "Compressing gene expression data using multiple latent space dimensionalities learns complementary biological representations," *Genome Biol.*, vol. 21, no. 1, pp. 1–27, May 2020, doi: 10.1186/s13059-020-02021-3.

[51] J. Bergstra, R. Bardenet, and Y. Bengio, "Algorithms for hyper-parameter optimization," in *Proc. Adv. Neural Inf. Process. Syst.*, vol. 24, 2011, pp. 2546–2554.

[52] Z. Yin and J. Hou, "Recent advances on SVM based fault diagnosis and process monitoring in complicated industrial processes," *Neurocomputing*, vol. 174, pp. 643–650, Jan. 2016, doi: 10.1016/j.neucom.2015.09.081.

[53] M. A. Hearst, S. T. Dumais, E. Osuna, J. Platt, and B. Scholkopf, "Support vector machines," *IEEE Intell. Syst. Appl.*, vol. 13, no. 4, pp. 18–28, Jul. 1998, doi: 10.1109/5254.708428.

[54] J. Zhang, J. Tian, A. M. Alcaide, J. I. Leon, S. Vazquez, L. G. Franquelo, H. Luo, and S. Yin, "Lifetime extension approach based on the Levenberg–Marquardt neural network and power routing of DC–DC converters," *IEEE Trans. Power Electron.*, vol. 38, no. 8, pp. 10280–10291, Aug. 2023, doi: 10.1109/TPEL.2023.3275791.

[55] M. Sokolova and G. Lapalme, "A systematic analysis of performance measures for classification tasks," *Inf. Process. Manage.*, vol. 45, no. 4, pp. 427–437, Jul. 2009, doi: 10.1016/j.ipm.2009.03.002.

[56] Y. Bengio, O. Delalleau, and N. Le Roux, "The curse of dimensionality for local kernel machines," Universite de Montreal, Montreal, QC, Canada, Tech. Rep. 1258, Mar. 2005.

[57] P. Vincent, H. Larochelle, I. Lajoie, Y. Bengio, and P. A. Manzagol, "Stacked denoising autoencoders: Learning useful representations in a deep network with a local denoising criterion," *J. Mach. Learn. Res.*, vol. 11, no. 12, pp. 3371–3408, Dec. 2010.

MINJAE KIM received the B.S. degree in mechanical engineering from Hanyang University, Seoul, South Korea, in 2022, where he is currently pursuing the M.S. degree in mechanical convergence engineering.

His research interests include explainable artificial intelligence for prognostics and prediction of remaining useful life.

SEHO SON received the B.S. degree in energy system engineering from Chung-Ang University, Seoul, South Korea, in 2020. He is currently pursuing the Ph.D. degree in mechanical convergence engineering with Hanyang University.

His research interests include data-driven prognosis and health management, and deep neural networks for remaining useful life estimation.

KI-YONG OH received the B.S. degree in mechanical engineering from Hanyang University, Seoul, South Korea, in 2005, the M.S. degree in mechanical engineering from the Korea Advanced Institute of Science and Technology (KAIST), in 2006, and the Ph.D. degree in mechanical engineering from the University of Michigan, Ann Arbor, MI, USA, in 2016.

In 2021, he joined the School of Mechanical Engineering, Hanyang University, where he is currently an Assistant Professor. His teaching and research interests include applied dynamics, and prognostics and health management in the field of complex energy systems.